

Collective dipole excitations in sodium clusters

A. A. Raduta,^{1,2} R. Budaca,² and Al. H. Raduta²

¹*Department of Theoretical Physics, Bucharest University, Bucharest POB MG11, Romania*

²*Institute of Physics and Nuclear Engineering, Bucharest POB MG6, Romania*

(Received 3 December 2008; published 13 February 2009)

Some properties of small and medium sodium clusters are described within the random-phase approximation (RPA) approach using a projected spherical single-particle basis. The oscillator strengths calculated with a Schiff-type dipole transition operator and folded with Lorentzian functions are used to calculate the photoabsorption cross-section spectra. The results are further employed to establish the dependence of the plasmon frequency on the number of cluster components. Static electric polarizabilities of the clusters excited in a RPA dipole state are also calculated. Comparison of our results with the corresponding experimental data shows an overall good agreement.

DOI: [10.1103/PhysRevA.79.023202](https://doi.org/10.1103/PhysRevA.79.023202)

PACS number(s): 36.40.Gk, 36.40.Vz, 36.40.Ei

I. INTRODUCTION

Although the field of metallic clusters is very old, it became very attractive for both theoreticians and experimentalists only since 1984, when the pioneering paper of Knight *et al.* [1] pointed out the electronic shells in alkali-metal clusters. Some notable contributions in the new era of the field have been reviewed by several authors [2–5].

The clusters which are most interesting to be studied seem to be those with a moderate number of atoms. Indeed, for such systems neither statistical models [6] nor *ab initio* quantum-chemical methods [7] are justified. Instead, the mean-field approach is vastly used. Several solutions defining the mean field for the single-particle motion have been employed along the years. Among them, three procedures are to be distinguished: (i) solving the Kohn-Sham equations [8]; (ii) assuming that the positive charge of the ionic core is uniformly distributed in a sphere of radius R . This is known in the literature as the jellium hypothesis [9,10]; (iii) postulating the average potential [11].

The researchers in this field paid attention especially to spherical clusters since in this shape are associated notions such as shell structure or magic numbers. However, there are some features such as the detailed structure of the abundance spectrum [12], or the split of plasmon energies [13–19], which cannot be explained assuming a spherical symmetry for the mean field. Moreover, measuring the split of the plasmon energy one can get information about the cluster deformation.

The first paper devoted to the deformed clusters was due to Clemenger [20] and published in 1985. The author adapts the Nilsson model formulated for nuclear systems [21], by ignoring the spin-orbit term. The resulting model is, therefore, referred to as the Clemenger-Nilsson (CN) model. The CN model was very successful in explaining several properties which depend on the cluster shape and which could not be described within a formalism using a mean field with spherical symmetry. The model is suitable to describe the single-particle properties in the intrinsic frame and especially for strong coupling regime when the wave function of the whole system can be factorized into an intrinsic part and a Wigner function accounting for the rotational degrees of

freedom. For clusters exhibiting an axial symmetry the projection of angular momentum on the symmetry axis denoted by K is a good quantum number. Of course the angular momentum itself is not a good quantum number. In view of the fact that the measurements are achieved in the laboratory frame where the rotation symmetry is valid we have to pay attention to this feature. Indeed, there are many properties which are very sensitive to the change in angular momentum of the system. Moreover in most cases K is not a good quantum number and therefore the factorization mentioned above is not possible. The typical case of this kind is that of systems with triaxial shapes. A many-body treatment of such situations would require a subsequent projection of the angular momentum. Such an operation is technically very difficult to achieve and to our knowledge up to now only approximate solutions have been adopted. In a previous publication, one of us (A.A.R.) proposed a solution for constructing a single-particle basis with good spherical symmetry and depending on deformation [22]. In the quoted work the model's ability to account in a realistic fashion for the main features of the deformed clusters has been successfully tested. Thus, the cluster shape, the magic numbers, and the supershell effects have been determined and a good agreement with the data as well as with the previous theoretical results has been obtained. For example, our results concerning the supershell structure are consistent with the picture described in the work of Nishioka *et al.* [11] as well as with the experimental data [23,24].

In a subsequent paper we continued the exploration of the deformed cluster properties, within the projected spherical basis introduced in Ref. [22]. The single-particle symmetry is actually the mean-field symmetry. This feature is an important property related to the charge distribution of the valence electrons. Such a structure becomes very important when one studies the response of the cluster to the action of an external electromagnetic field.

Guided by a possible parallelism between atomic clusters and nuclear systems pointed out in Refs. [25,26], in Ref. [27] one of us (A.A.R.) studied, in collaboration, properties such as skin structure, empty center, hard center, cluster subsystems, and halo behavior. Such properties have been seen, indeed, in the structure of the charge density function. Based on phenomenological arguments, quantitative results for po-

larizability and plasmon frequency have been derived.

In this paper we study the collective many-body properties of light and medium sodium clusters. The paper is structured as follows. In Sec. II we briefly review the projected single-particle basis. In Sec. III the basic equations specific to the particle-hole (p - h) random-phase approximation (RPA) are written down. The RPA wave functions are used in Sec. IV to treat the electric dipole transitions and the photoabsorption cross section. In the framework of p - h RPA the expressions for system polarizability are analytically derived in Sec. V. Numerical applications for Na clusters with the number of components varying from 6 to 40 have been performed and the results are described in Sec. VI. The final conclusions are summarized in Sec. VII.

II. PROJECTED SPHERICAL SINGLE-PARTICLE BASIS

We restrict our considerations to the energy domain of laser beam experiments (i.e., optical domain) where only the valence electrons may be excited and delocalized, the remaining ones defining the atomic core. Under these circumstances we could study those atomic cluster properties which are mainly determined by the valence electrons. The picture is even more simplified if the cluster building block is an alkali metal. In this case the interacting system of electrons and positively charged ions is replaced by a system of interacting electrons moving in a mean field which accounts for the influence of the ionic core on the single-particle motion. Each atom of a given cluster is represented by one valence electron.

In a previous publication [22], the mean field for the valence electrons was defined with the help of a model Hamiltonian associated to the particle-core interacting system,

$$\begin{aligned}
 H &= \frac{p^2}{2m} + \frac{m\omega_0^2 r^2}{2} - D(l^2 - \langle l^2 \rangle) + H_c \\
 &\quad - m\omega_0^2 r^2 \sum_{\lambda=0,2} \sum_{-\lambda \leq \mu \leq \lambda} \alpha_{\lambda\mu}^* Y_{\lambda\mu} \\
 &\equiv H_p + H_c + H_{pc},
 \end{aligned} \tag{2.1}$$

where $\alpha_{\lambda\mu}$ are λ -pole shape variables defining the deformed ionic core through the surface equation

$$R = R_0 \left[1 + \sum_{\lambda=0,2} \sum_{-\lambda \leq \mu \leq \lambda} \alpha_{\lambda\mu}^* Y_{\lambda\mu}(\theta, \phi) \right]. \tag{2.2}$$

The volume conservation condition allows us to relate the monopole and quadrupole coordinates:

$$\alpha_{00} = - \frac{1}{\sqrt{4\pi}} \sum_{-2 \leq \mu \leq 2} |\alpha_{2\mu}|^2. \tag{2.3}$$

For what follows it is convenient to introduce the boson operators $b_{2\mu}^\dagger$:

$$\alpha_{2\mu} = \frac{1}{k\sqrt{2}} [b_{2\mu}^\dagger + (-1)^\mu b_{2-\mu}], \tag{2.4}$$

$$\pi_{2\mu} = \frac{ik}{\sqrt{2}} [-b_{2\mu} + (-1)^\mu b_{2-\mu}^\dagger].$$

The core subsystem is considered to be a harmonic quadrupole boson Hamiltonian:

$$H_c = \omega_c \sum_{\mu} b_{2\mu}^\dagger b_{2\mu}. \tag{2.5}$$

Let us consider the coherent state

$$|\Psi_c\rangle = \exp[d(b_{20}^\dagger - b_{20})]|0\rangle, \tag{2.6}$$

where $|0\rangle$ denotes the vacuum state of quadrupole bosons. This wave function is a coherent state,

$$b_{2m} |\Psi_c\rangle = \delta_{m0} d |\Psi_c\rangle, \tag{2.7}$$

and describes the ground state of a deformed quadrupole boson Hamiltonian. Moreover, the expected value of the static quadrupole moment in the state $|\Psi_c\rangle$ is proportional to d . Due to this feature, d is referred to as *the deformation parameter*.

Note that averaging H with $|\Psi_c\rangle$, we obtain a deformed single-particle mean field which is similar to that used by Clemenger in Ref. [20]. On the other hand, averaging H with an eigenstate $|nlm\rangle$ of H_p , one arrives at a deformed quadrupole boson Hamiltonian which admits $|\Psi_c\rangle$ as ground state if a suitable deformation parameter is chosen. These properties suggest that the particle-core system wave function might be described by a transformation applied to the product function with the factors $|nlm\rangle$ and $|\Psi_c\rangle$.

The deformation of the single-particle mean field in Clemenger's model, δ , might be related to the deformation parameter d involved in the coherent state defined above. Aiming for this goal, we require that the average of H_{pc} with $|\Psi_c\rangle$ is identical to the deformed single-particle potential from Clemenger's Hamiltonian. This supplies us with the relation

$$\frac{d}{k} = \sqrt{\frac{2\pi}{45}} (\Omega_\perp^2 - \Omega_z^2), \tag{2.8}$$

where Ω_z and Ω_\perp denote the frequencies along and perpendicular to the symmetry axis, respectively. This relation yields a simple equation for the two deformation parameters:

$$0.693k\delta = d. \tag{2.9}$$

In our calculations, the adopted value for the constant k , defining the canonical transformation (2.4), is 9.77. The mean field defines an intrinsic frame of reference for electrons. In the laboratory frame the system is described by states having good angular momentum due to the rotation symmetry of the model Hamiltonian. A basis in the laboratory frame for the composite system, of electrons and core, may be obtained by diagonalizing H in a particle-core product basis, with components of definite angular momenta. However, to use such a basis in a RPA formalism is quite a tedious task.

A great simplification is obtained if, instead, we use a projected spherical single-particle basis. Obviously, even if the deformed set of generating functions is orthogonal the

angular momentum projected set is not orthogonal. Fortunately, an orthogonal set of projected states is obtained if we choose an appropriate single-particle state factor.

Thus, it can be proved that the following subset of projected states is orthogonal:

$$\begin{aligned}\phi_{IM;\sigma}(nl;d) &= \mathcal{N}_{nl}^I(d) [P_{MI}^I |nlI\rangle \Psi_c(d)] \chi_\sigma, \\ &\text{for } I \neq 0, l = \text{even}, \\ \phi_{00;\sigma}(nl;d) &= \mathcal{N}_{nl}^0(d) [P_{00}^0 [|nl\rangle \hat{s}]_{l+1,0} \Psi_c(d)] \chi_\sigma, \\ &\text{for } I = 0, l = \text{odd},\end{aligned}\quad (2.10)$$

where \hat{s} denotes the spin operator and χ_σ is the bispinor component. The standard notation for the angular momentum projection operator was used:

$$P_{MK}^I = \frac{2I+1}{8\pi^2} \int D_{MK}^{I*}(\Omega) \hat{R}(\Omega) d\Omega. \quad (2.11)$$

The norms $\mathcal{N}_{nl}^I(d)$ of these projected states are

$$\begin{aligned}[\mathcal{N}_{nl}^I]^{-2} &= \sum_J (C_{IJ}^{I0I})^2 (N_J^{(c)})^{-2}, \quad \text{for } I \neq 0, l = \text{even}, \\ [\mathcal{N}_{nl}^0]^{-2} &= \frac{1}{4} \frac{1}{2l+3} (N_{l+1}^{(c)})^{-2}, \quad \text{for } I = 0, l = \text{odd},\end{aligned}\quad (2.12)$$

with $N_J^{(c)}$ denoting the norm of the J component projected from the deformed state $|\Psi_c\rangle$ describing the core. If one neglects the matrix elements with $\Delta l = \pm 2$ and $\Delta n = 2$, the eigenvalues of H within the projected spherical basis can be fairly well approximated by the average values:

$$\begin{aligned}\epsilon_{nl}^I(d) &\equiv \langle \phi_{IM;\sigma}(nl;d) | H | \phi_{IM;\sigma}(nl;d) \rangle \\ &= \hbar\omega_0 \left(N + \frac{3}{2} \right) - D \left[l(l+1) - \frac{N(N+3)}{2} \right] + \hbar\omega_0 \left(N + \frac{3}{2} \right) \\ &\quad \times \frac{1}{90} (\Omega_\perp^2 - \Omega_z^2)^2 \left[1 + \frac{1}{d^2} \left\langle \sum_\mu b_{2\mu}^\dagger b_{2\mu} \right\rangle \right] \\ &\quad - \hbar\omega_0 \left(N + \frac{3}{2} \right) \frac{1}{3} (\Omega_\perp^2 - \Omega_z^2) F_{II}.\end{aligned}\quad (2.13)$$

The expected value of the boson number operator as well as the factor F_{II} was calculated analytically in Ref. [22]. The energies $\epsilon_{nl}^I(d)$ depend on d in the same manner as the single-particle energies in Clemenger's model depend on the deformation δ . This comparison has been performed in Ref. [22]. The deformation parameter is fixed so that the cluster energy is minimum against any variation in d .

As shown in Ref. [28], although the functions are characterizing a particle-core system, they can be used to describe a many fermion system. Indeed, in calculating the matrix elements of a one-body operator, one integrates first on the core coordinates and then on single-particle coordinates. Finally, the matrix element is written in a factorized form, one factor describing the matrix elements between spherical wave func-

tions and the other one carrying the dependence on the deformation. Moreover, due to the specific properties of the coherent state the projected spherical states can be used for calculating the matrix elements of a two-body operator. Indeed, in Ref. [29] we have proved that the matrix elements of a two-body interaction are practically equal to the matrix elements between states projected from the product of two particle states and a common core's coherent state.

To conclude the single-particle energies are approximated by those given in Eq. (2.13) while the corresponding wave functions are approximated by Eqs. (2.10) and (2.12). Actually, these are input data for the treatment of a many-body Hamiltonian associated with a system of interacting valence electrons moving in the mean field presented above.

III. RPA DESCRIPTION OF THE COLLECTIVE DIPOLE STATES

We assume that the valence electrons moving in the mean field of the ionic core and interacting among themselves through a Coulomb force are described by the model Hamiltonian

$$H = H_{\text{mf}} + V_C, \quad (3.1)$$

which is a sum of the static self-consistent, single-particle Hamiltonian H_{mf} and of the two-body residual Coulomb interaction V_C . The residual two-body interaction is given, in the local-density approximation (LDA), by

$$V(\vec{r}_1 - \vec{r}_2) = \frac{e^2}{|\vec{r}_1 - \vec{r}_2|} + \frac{dV_{\text{XC}}[\rho]}{d\rho} \delta(\vec{r}_1 - \vec{r}_2). \quad (3.2)$$

The quantity $V_{\text{XC}} = d\varepsilon_{\text{XC}}[\rho]/d\rho$ is the exchange-correlation potential in the ground state. We use the exchange-correlation energy density ε_{XC} of Gunnarsson and Lundqvist [30] as in Refs. [31,32]. Thus, the following expression for the exchange-correlation potential V_{XC} given in atomic units is obtained:

$$V_{\text{XC}}(\vec{r}) = -\frac{1.222}{r_s(\vec{r})} - 0.0666 \ln\left(1 + \frac{11.4}{r_s(\vec{r})}\right). \quad (3.3)$$

Here $r_s(\vec{r}) = [3/4\pi\rho(\vec{r})]^{1/3}$ is the local value of the Wigner-Seitz radius. The two-body interaction is expanded in multipoles, the λ -pole term having the expression [31]:

$$V(r_1, r_2; \lambda) = e^2 \frac{r_{<}^\lambda}{r_{>}^{\lambda+1}} + \frac{dV_{\text{XC}}[\rho]}{d\rho} \frac{\delta(r_1 - r_2)}{r_1^2} \frac{2\lambda + 1}{4\pi}, \quad (3.4)$$

where $r_{<} = \min(r_1, r_2)$ and $r_{>} = \max(r_1, r_2)$.

For $\lambda = 1$, the two-body interaction has the expression

$$\begin{aligned}V(r_1, r_2; \lambda = 1) &= e^2 \frac{r_1}{r_2^2} + F(\rho, r_s) \frac{\delta(r_1 - r_2)}{r_1^2}, \\ F(\rho, r_s) &= -\frac{1}{4\pi\rho r_s} \left[1.222 + \frac{0.759 r_s}{r_s + 11.4} \right].\end{aligned}\quad (3.5)$$

The one-body term represented by the mean field H_{mf} and the ($\lambda = 1$)-pole term of the two-body interaction are treated within the RPA formalism which defines an operator

$$C_{1\mu}^\dagger = \sum_{ph} [X_{ph}(c_p^\dagger c_h)_{1\mu} - Y_{ph}(c_h^\dagger c_p)_{1\mu}], \quad (3.6)$$

subject to the restrictions

$$[H, C_{1\mu'}^\dagger] = \hbar\omega C_{1\mu'}^\dagger, \quad (3.7)$$

$$[C_{1\mu}, C_{1\mu'}^\dagger] = \delta_{\mu,\mu'}. \quad (3.8)$$

Written in a matricial form, the RPA equations provided by Eq. (3.7) look like

$$\begin{pmatrix} A & B \\ -A^* & -B^* \end{pmatrix} \begin{pmatrix} X^n \\ Y^n \end{pmatrix} = \hbar\omega_n \begin{pmatrix} X^n \\ Y^n \end{pmatrix}. \quad (3.9)$$

The submatrices A and B have the expressions

$$\begin{aligned} A(ph; p'h') &= (\varepsilon_p - \varepsilon_h) \delta_{p,p'} \delta_{h,h'} - B(ph; p'h'), \\ B(ph; p'h') &= 2 \frac{\hat{I}_p \hat{I}_h \hat{I}_{p'} \hat{I}_{h'}}{3} C_{000}^{l_h l_p} C_{000}^{l_{h'} l_{p'}} f_{l_p l_h}^{p'h'}(d) \\ &\quad \times f_{l_{p'} l_{h'}}^{p'h'}(d) R(ph'; hp'), \end{aligned} \quad (3.10)$$

where

$$\begin{aligned} R(ph'; hp') &= \int r_1^2 dr_1 r_2^2 dr_2 \mathcal{R}_{n_p l_p}(r_1) \\ &\quad \times \mathcal{R}_{n_h l_h}(r_2) V(r_1, r_2; 1) \mathcal{R}_{n_{h'} l_{h'}}(r_1) \mathcal{R}_{n_{p'} l_{p'}}(r_2), \end{aligned} \quad (3.11)$$

with $\mathcal{R}_{n_l l_l}(r)$ being the radial part of the single-particle projected wave functions. Since the two-body interaction consists of two terms, the Coulomb and the exchange term, correspondingly the factor $R(ph'; hp')$ splits into two parts which are given in the Appendix. The factor 2 of the submatrix B accounts for the spin degeneracy.

The factor $f(d)$ carrying the dependence on deformation parameter d , involved in Eq. (3.10), has the expressions given in the Appendix. Equation (3.9) determines the amplitudes X and Y up to a multiplicative constant which is fixed by the normalization condition (3.8):

$$\sum_{p,h} [|X_{ph}^n|^2 - |Y_{ph}^n|^2] = 1. \quad (3.12)$$

The compatibility condition for the set of equations (3.9) is an equation for ω . The number of solutions, for the RPA equations, is equal to the number of dipole particle-hole (p - h) configurations, hereafter denoted by N_s . To the solution $\hbar\omega_k$, the amplitudes X_{ph}^k and Y_{ph}^k correspond. These amplitudes characterize the phonon operator $C_{1\mu}^\dagger(k)$ which may excite the cluster ground state $|0\rangle$ to a one-phonon state:

$$C_{1\mu}(k)|0\rangle = 0, \quad |1_k\mu\rangle = C_{1\mu}^\dagger(k)|0\rangle. \quad (3.13)$$

There are several procedures to solve numerically the RPA equations. Here we have adopted the method proposed by Ullah and Rowe in Ref. [33].

Concerning the RPA description, we would like to comment on the following features:

(a) Due to its specific structure, the state with $I=0$ and $l=\text{odd}$ may be related, by the p - h dipole operator, to states with either the spin up or the spin down. Consequently the RPA matrix does not have a decoupled block structure, each block being characterized by a unique orientation of the electron spin. The coupling terms are, however, small and bring negligible contribution. For this reason we ignore from the beginning the terms which flip the spin of the p - h matrix elements.

(b) In the definition of the phonon operator (3.6) the summation involves both states (2.10) with the factor state $\chi_{1/2}$ and with the bispinor $\chi_{-1/2}$. We, conventionally, call the resulting operator as *the extended phonon operator*. In virtue of (a) we may restrict the summation to one component and therefore work with the so-called *reduced phonon operator*. The normalization to unity of the two phonon operators suggests a simple relationship between their defining amplitudes.

In our approach the reduced phonon operator has been used, otherwise the degeneracy of the states with spin up and with spin down has been carefully implemented whenever the matrix elements between RPA states were calculated.

IV. E1 TRANSITIONS AND PHOTOABSORPTION CROSS SECTION

The reduced probability for the dipole transition $|0\rangle \rightarrow |1_n^+\rangle$ can be written as¹

$$B(E1, 0^+ \rightarrow 1_n^+) = |\langle 0 | \mathcal{M}(E1) | 1_n^+ \rangle|^2, \quad (4.1)$$

where

$$\langle 0 | \mathcal{M}(E1) | 1_n^+ \rangle = \sum_{p,h} \hat{I}_p \langle p | \mathcal{M}(E1) | h \rangle [X_{ph}^n + (-1)^{l_p+l_h} Y_{ph}^n] \quad (4.2)$$

are the reduced matrix elements of the dipole operator $\mathcal{M}(E1)$ between the specified RPA state. The one-phonon state $|1_n\rangle$ is characterized by the RPA amplitudes X_{ph}^n and Y_{ph}^n obtained by solving Eq. (3.7).

Instead of the usual transition dipole operator, we make use of a modified operator which is similar to the so-called Schiff moment from nuclear physics [34]:

$$\mathcal{M}(E1) = \sqrt{\frac{4\pi}{3}} e \mathcal{Y}_{1\mu}(\Omega) \left(r - \frac{3}{5} \frac{r^3}{r_s^2} \right). \quad (4.3)$$

Here r_s is the Wigner-Seitz radius and is equal to 3.93 (a.u.) for Na clusters. The corrective component, involved in the dipole operator, relates particle and hole states characterized by $\Delta N=3$, which results in modifying the strength distribution among the RPA states. Such an effect is obtained in a natural manner, i.e., using the standard form for the dipole transition operator, if the mean-field potential for the single-particle motion involves higher powers of the radial coordinate.

¹Throughout this paper Rose's convention for the reduced matrix elements is used.

We define the oscillator strength f_n per atom as

$$f_n = \frac{\hbar \omega_n B(E1, 0^+ \rightarrow 1_n^+)}{S(E1)}, \quad (4.4)$$

where ω_n is the RPA excitation energy corresponding to the n th—order solution of RPA equation, and

$$S(E1) = \sum_n \hbar \omega_n B(E1, 0^+ \rightarrow 1_n^+), \quad (4.5)$$

such that $\sum_n f_n = 1$.

To calculate the photoabsorption cross section per atom, $\sigma(\omega)$, one folds the oscillator strengths, which are just vertical straight lines, with Lorentzian shapes normalized to unity as follows:

$$\sigma(\omega) = C \sum_n f_n L(\omega; \omega_n, \Gamma_n), \quad (4.6)$$

where $\hbar \Gamma_n$ denotes the full widths at half maximum of the Lorentzian profiles and is provided by fixing the damping factor $\gamma = \Gamma/\omega$, with $\hbar \omega_r$ being the energy of the resonance peak. This damping factor varies, in our calculation, in the range of 0.06–0.135 [35] which is appropriate for the room temperature. Indeed, the damping factor is considered to be caused by the coupling of the electronic dipole oscillation to the thermal fluctuations of the cluster surface [35,36]. The thermal mechanism of broadening the plasmon line was first considered in Ref. [36]. Therein the plasmon line is a Gaussian while in Ref. [35] the plasmon profile is described by a Lorentzian function. Note that the RPA calculations provide a line broadening due to the fragmentation of the collective strength onto near-lying excitations of a one-electron one-hole nature. This effect is temperature independent and is referred to as the Landau damping.

The proportionality coefficient C , in Eq. (4.6), is given by

$$C = \frac{2\pi^2 e^2 \hbar}{m_e c} = 1.0975 (\text{eV } \text{\AA}^2). \quad (4.7)$$

This value is obtained by normalizing the photoabsorption cross section such that the area per delocalized electron under the photoabsorption curve is constant [37],

$$\int_0^\infty \sigma(\omega) d(\hbar\omega) = \frac{2\pi^2 e^2 \hbar}{m_e c}, \quad (4.8)$$

which is consistent with the value of the dipole sum rule. Note that the results for the reduced $E1$ transition probability as well as for the photoabsorption cross section depend on the single-particle features specified by the mean-field parameter $\hbar \omega_0$. The oscillator parameter of energy quanta $\hbar \omega_0$ depends on the cluster atoms number as $E_F/\mathcal{N}^{1/3}$, where E_F is the Fermi energy, which is about 3 eV for a spherical cluster. However, in general, E_F is not the same for all clusters. Keeping this in mind, we use a Fermi energy $E_F(\mathcal{N})$ which also depends on the number of cluster's atoms. The \mathcal{N} dependence is extracted by interpolating the results provided by a least-squares fit for the experimental photoabsorption cross-section spectrum. In our calculations one also needs to know the oscillator length b . This depends on the choice of

oscillator energy quanta, and therefore exhibits the \mathcal{N} dependence given by $b = [\hbar^2/m_e E_F(\mathcal{N})]^{1/2} \mathcal{N}^{1/6}$.

V. ELECTRIC POLARIZABILITY

In the classical picture, the static electric polarizability of a jellium metal sphere of radius R has the expression

$$\alpha_0 = R^3, \quad (5.1)$$

where R , given in terms of the Wigner-Seitz radius r_s , is $R = r_s \mathcal{N}^{1/3}$.

Quantum-mechanical effects determine corrections to the classical results for plasmon energy and polarizabilities. The electron density is not going sharply to zero at the cluster surface but reduces gradually at the surface and moreover extends significantly beyond to jellium edge. The spill-out electrons produce a screening effect against external fields which results in changing the classical result for polarizability to

$$\alpha = (R + \Delta)^3. \quad (5.2)$$

The radius shift Δ can be expressed in terms of the fraction of the total number of electrons which are spilled out of the jellium sphere and the final result for the static polarizability reads

$$\alpha = R^3 \left(1 + \frac{\mathcal{N}_{\text{sp}}}{\mathcal{N}} \right), \quad (5.3)$$

where \mathcal{N}_{sp} denotes the number of spilled-out electrons. Actually, this is a reasonable approximation of the result predicted by the sum rule S_{-2} [4,5,38],

$$\alpha = R^3 \left(1 - \frac{\mathcal{N}_{\text{sp}}}{\mathcal{N}} \right)^{-1}. \quad (5.4)$$

This expression is obtained by using the relationship between the plasmon redshift and the electric polarizability, provided by the moment S_{-2} . Also one assumes that the entire oscillator strength is concentrated near the surface plasmon, i.e., one ignores the presence of the volume plasmon, which allows us to use the result for the Thomas-Reiche-Kuhn sum rule S_0 .

We propose a method for obtaining the number of spill-out electrons by means of the RPA formalism, using the RPA eigenstates for computing the average value of number of particles operator $\hat{N} = \sum_i c_i^\dagger c_i$, where the summation run over all particle and hole states. Thus the operator to be averaged is given by

$$\hat{N} = \sum_p c_p^\dagger c_p + \sum_h c_h^\dagger c_h. \quad (5.5)$$

The averaging operation will be constrained by the condition that the radial integrals from all scalar products involved will have the limits $[R, \infty)$, instead of $[0, \infty)$, where $R = r_s \mathcal{N}^{1/3}$ is the radius of the metal sphere which is supposed to contain all electrons. In this manner we will get the average number of electrons which are beyond this sphere. The particle number operator can be written in a second quantization likeform

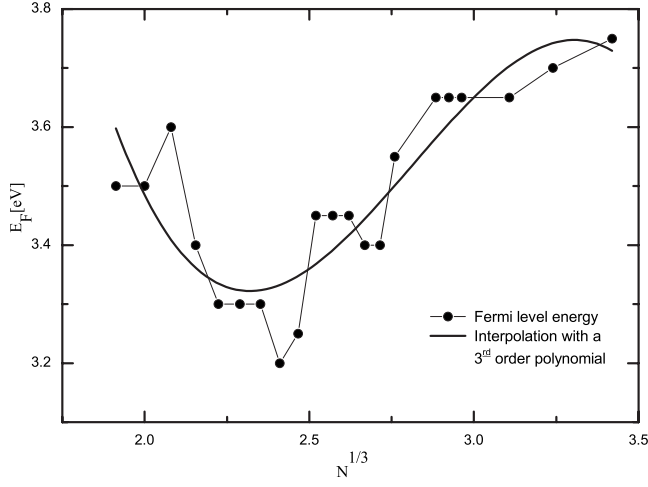


FIG. 1. The Fermi energies (black circles), which reproduce the experimental photoabsorption cross-section spectra, are interpolated with a third-order polynomial in $N^{1/3}$: $E_F(N) = -0.886466N + 7.47916N^{2/3} - 20.3871N^{1/3} + 21.4339$.

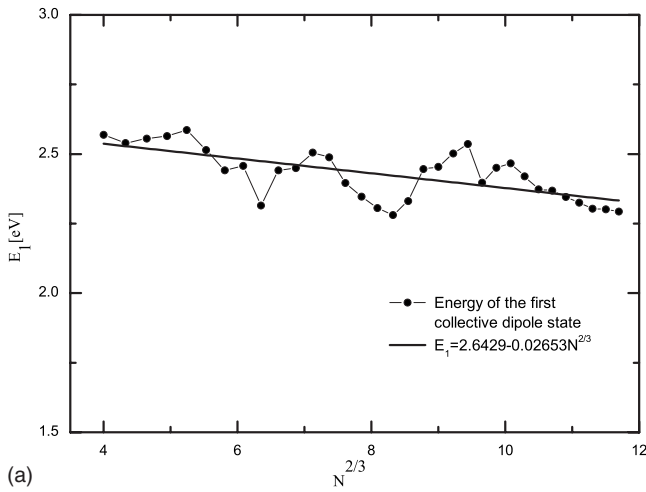
$$\hat{N} = \sum_{kk'} \langle C_{1\mu}(k) | \hat{N} | C_{1\mu}^\dagger(k') \rangle C_{1\mu}^\dagger(k) C_{1\mu}(k'). \quad (5.6)$$

Averaging \hat{N} with the RPA eigenstates we get

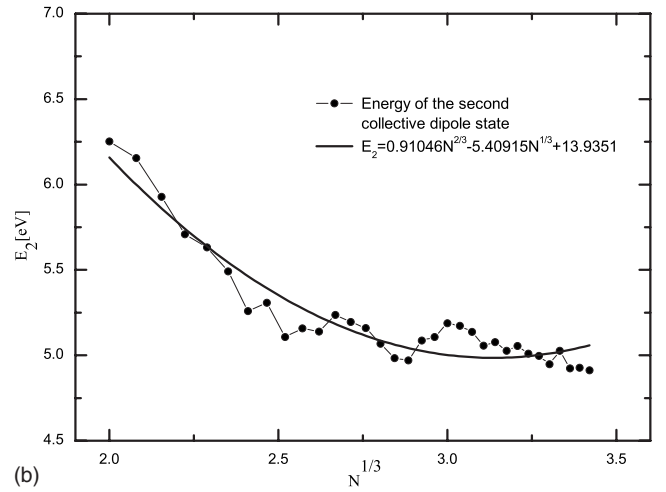
$$\langle \hat{N} \rangle = \sum_k \langle C_k | \hat{N} | C_k^\dagger \rangle = 2 \sum_k \sum_{ph} \{ [\nu(I_p) X_{ph}^k f_p^R]^2 + [\nu(I_h) Y_{ph}^k f_h^R]^2 \}. \quad (5.7)$$

Here, the overlap of two single-particle projected functions corresponding to two particles or two holes states is expressed through the product of the statistical factor $\nu(I_i)$ and the radial integral

$$f_i^R = \int_R^\infty [\mathcal{R}_{n_l i}(r)]^2 r^2 dr, \quad i = p, h. \quad (5.8)$$



(a)



(b)

FIG. 2. (a) The RPA energy of the first collective dipole state decreases very slowly and almost linearly in $N^{2/3}$. (b) For the second collective dipole state the energy is decreasing faster by means of a parabolic law in $N^{1/3}$. Theoretical results for all the clusters in the range of 8–40 atoms constituents are presented.

VI. NUMERICAL RESULTS

First, we identify the dependence of the Fermi energy on the number of atoms in cluster. The adopted procedure is as follows. For each cluster we determine the Fermi energy which corresponds to the best agreement of the calculated photoabsorption curve with the experimental points. Further, the obtained values are interpolated with a third-order polynomial in $N^{1/3}$ (see Fig. 1). The polynomial obtained in this way determines a Fermi energy varying in the range of 3.3–3.75 eV. The RPA calculations make use of the Fermi energies lying on the interpolating curve. In this way the RPA results depend on the number of atoms, by means of the oscillator energy quanta $\hbar\omega_0 = E_f(N)/N^{1/3}$ and the oscillator length $b = \sqrt{\hbar/m_e\omega_0}$.

The RPA calculations are performed for the restricted subspace of the particle-hole excitations, including only the $\Delta N=1$ and $\Delta N=3$ transitions. We use the method described in Ref. [33] to solve the RPA equations with real submatrices $A(ph;p'h')$ and $B(ph;p'h')$. The single-particle energies ε_i involved in the expression of the submatrix $A(ph;p'h')$ are provided by formula (2.13). Once the RPA amplitudes and energies are determined, the electric dipole transition probabilities and the oscillator strengths can be computed by means of Eqs. (4.1) and (4.4). The biggest values for the transition probabilities define the collective states. The corresponding RPA energies are located mainly in two regions associated with the first collective dipole state, with the major contribution coming from the $\Delta N=1$ excitations, and the second collective dipole state, which is due to the $\Delta N=3$ transitions. The energy of the state characterized by a dominant transition probability varies from one cluster to another. Thus, the energies of the first and second collective states depend on $N^{2/3}$ and $N^{1/3}$, respectively, as shown in Fig. 2. Therefore, the first collective state seems to have a surface mode behavior, while the second collective excitation exhibits both a surface and a volume feature. In a short interval of N the volume character of the collective dipole mode of larger energy prevails.

TABLE I. The dominant RPA X_{ph} amplitudes of the first collective dipole states achieved by $\Delta N=1$ transitions for some of the Na clusters. The corresponding dipole p - h configuration as well the RPA energies are also mentioned. Note that the heavier the clusters are the more collective is the depicted RPA mode. Also due to the repulsive character of the two-body interaction the order of the RPA root is increasing with N despite the fact that the energy is slightly decreasing.

Cluster	$[NII]_h \rightarrow [NII]_p$	X_{ph}^k	Y_{ph}^k	Solution's order k	$\hbar\omega_k$ (eV)
Na ₈	$[111]_h \rightarrow [222]_p$	0.7154	0.1525	5	2.569
	$[111]_h \rightarrow [200]_p$	0.6297	0.0636		
	$[110]_h \rightarrow [221]_p$	-0.3416	-0.0723		
Na ₁₄	$[220]_h \rightarrow [311]_p$	0.8795	0.0103	9	2.619
	$[221]_h \rightarrow [311]_p$	-0.2628	-0.0131		
	$[111]_h \rightarrow [222]_p$	0.2339	0.0611		
	$[221]_h \rightarrow [332]_p$	0.2044	0.0568		
	$[220]_h \rightarrow [331]_p$	0.1837	0.0600		
	$[111]_h \rightarrow [200]_p$	0.1396	0.0384		
	$[221]_h \rightarrow [331]_p$	0.1309	0.0514		
Na ₁₈	$[220]_h \rightarrow [331]_p$	0.4709	0.1611	12	2.449
	$[222]_h \rightarrow [333]_p$	0.4354	0.1492		
	$[111]_h \rightarrow [200]_p$	0.4213	0.0928		
	$[221]_h \rightarrow [332]_p$	0.4211	0.1441		
	$[221]_h \rightarrow [331]_p$	0.3847	0.1315		
	$[222]_h \rightarrow [311]_p$	0.3635	0.0635		
	$[221]_h \rightarrow [310]_p$	-0.1623	-0.0312		
Na ₂₀	$[200]_h \rightarrow [311]_p$	-0.5047	-0.1444	12	2.488
	$[220]_h \rightarrow [331]_p$	-0.4536	-0.1621		
	$[222]_h \rightarrow [333]_p$	-0.4194	-0.1501		
	$[221]_h \rightarrow [332]_p$	-0.4056	-0.1450		
	$[221]_h \rightarrow [331]_p$	-0.3705	-0.1323		
	$[222]_h \rightarrow [311]_p$	-0.3432	-0.0657		
	$[221]_h \rightarrow [310]_p$	-0.1623	-0.0312		
Na ₄₀	$[331]_h \rightarrow [442]_p$	-0.4117	-0.1681	22	2.293
	$[311]_h \rightarrow [422]_p$	-0.4075	-0.1369		
	$[311]_h \rightarrow [400]_p$	-0.4040	-0.0993		
	$[332]_h \rightarrow [443]_p$	-0.3182	-0.1298		
	$[331]_h \rightarrow [420]_p$	-0.2902	-0.0547		
	$[332]_h \rightarrow [421]_p$	-0.2593	-0.0489		
	$[331]_h \rightarrow [421]_p$	0.2391	0.0446		
$[330]_h \rightarrow [441]_p$	0.2326	0.0942			
$[310]_h \rightarrow [421]_p$	0.1947	0.0648			
$[332]_h \rightarrow [442]_p$	-0.1673	-0.0689			

In Table I, we collected the RPA amplitudes X_{ph} and Y_{ph} associated with the first collective dipole states in some Na clusters. From there one sees that notable contributions are brought by several particle-hole configurations, which contrasts the situation of the noncollective states where a certain component is by far dominant, while the others are negligible.

In order to compare the predictions of the present formalism with the experimental results for photoabsorption cross

sections, we have also to take into account the coupling of the electronic dipole oscillations with the thermal fluctuations of the cluster surface [13,35,36]. In the generalized picture, the photoabsorption cross section per atom for a spherical cluster that is much smaller than the photon wavelength [39] has the plasmon energy dependence

$$\sigma(\omega) = 4\pi \frac{e^2}{m_e \hbar c} \frac{\omega^2 \Gamma}{[\omega^2 - \omega_r^2]^2 + \omega^2 \Gamma^2}, \quad (6.1)$$

where Γ is an averaging parameter [35]. Here *the surface plasmon pole approximation* has been adopted. The resonance energy was denoted by $\hbar\omega_r$ while $\hbar\Gamma$ is just the resonance width. Keeping close to the general description of the photoabsorption cross section, the above formula can be simulated approximately by folding one oscillator strength line, predicted by the RPA calculation with a Lorentzian function displaying a damping factor $\gamma = \Gamma/\omega_r \approx 0.1$, which is appropriate for room temperature. This procedure is extended to folding all the strengths provided by the RPA calculation according to Eq. (4.6). Indeed, to each energy $\hbar\omega_k$ one associates a Lorentzian centered in $\hbar\omega_k$ and having a width given by the product of a constant damping factor γ and the Lorentzian resonance energy. In Fig. 3 theoretical curves of photoabsorption cross section per atom are displayed versus the wavelength, for several clusters for which experimental data are known in a large interval. Note that the RPA energies were given in terms of the corresponding wavelength $\lambda = 2\pi\hbar c/\omega_k$. Apart from some discrepancies in the form of the curves, such as plateaus or number of peaks, the present RPA calculations provide an overall good agreement with the experimental measurements in the visible range of energies. An interesting shape of the photoabsorption cross section is obtained for Na₁₄ cluster, which has a triaxial shape reflected in the fragmentation of the oscillator strength spectrum into three comparable peaks. These three distinct peaks are identified as plasmon frequencies associated with those three axes which define the triaxiality of the cluster. In a spherical cluster like Na₈ and Na₂₀ these three frequencies are degenerate which results in having only one peak in the photoabsorption cross-section curves. Also, our calculation predicts the double peak structure of photoabsorption spectra for clusters Na₁₀, Na₁₁, and Na₁₂. Actually this structure suggests an axially symmetric shape.

The photoabsorption spectrum for the clusters Na_N, with $N \leq 40$, has been measured in Refs. [13,14]. Therein, the measured data are interpreted within the ellipsoidal shell model (ESM) formalism. Although, at first glance, the curves presented in the quoted references and here look similar, there are some differences which are to be mentioned. For Na₂₀ the shape is quite well reproduced by our formalism while the predictions for the peak height and energy given in Ref. [14] are quite different from the corresponding experimental data. Concerning Na₈, both formalisms predict a resonance energy which is smaller than the experimental one. In our approach the ascending branch of the experimental curve is well reproduced, but the descending one exhibits a deviation due to the small value for the relative width parameter. For Na₁₂ the first two experimental peaks correspond to one

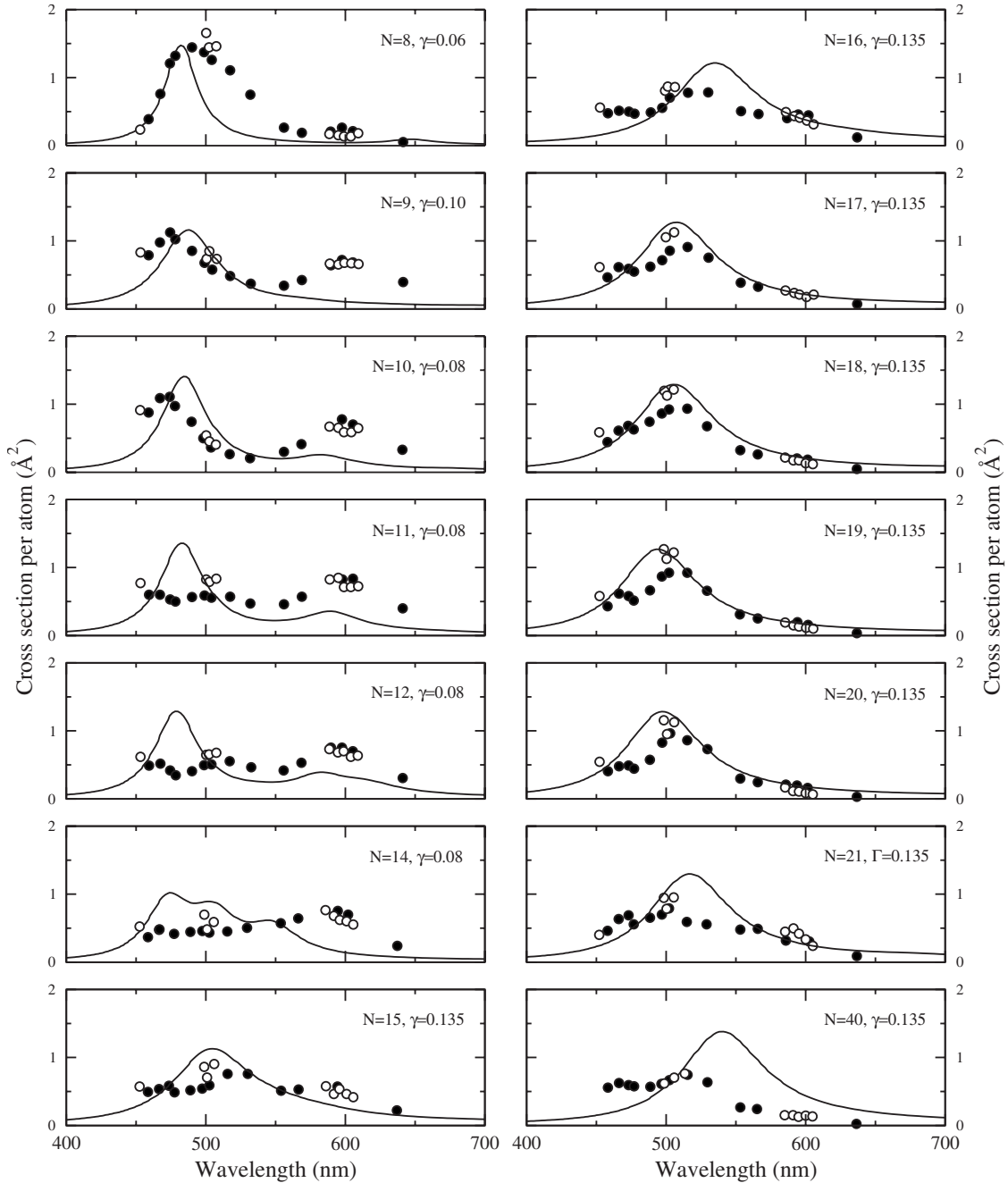


FIG. 3. Experimental (circles) and calculated (solid lines) photoabsorption cross sections vs wavelength for Na clusters of small and medium sizes. The experimental points are taken from Ref. [14], where the open circles correspond to data taken with a flash-lamp laser and have about 20% statistical errors. Solid circles have smaller statistical errors, about 5%–10%, for which cw lasers were used. The calculated curves are resulting from the folding of the RPA oscillator strengths with Lorentzian shapes normalized to unity. The Lorentzian shapes are specified by the relative width parameter $\gamma = \Gamma / \omega_r$, which varies from one cluster to another in the range of 0.06–0.135, $\hbar \omega_r$ being the peak energy of a given Lorentzian.

large peak in our calculations. For Na_{14} we predict a triaxial shape reflected in the three peaks shown in Fig. 3, while in Ref. [14] only one peak is noticed. For Na_N with $17 \leq N \leq 21$, our calculations describe the experimental data better than ESM. As for Na_{40} both formalisms predict a broad line with a peak which is higher than that shown by the data. The centroid energy calculated in the present paper is higher than the measured resonance energy, while in Ref. [14] the

centroid energy is smaller. A possible cause for the differences mentioned above is the use of different single-particle bases in the two approaches.

Taking a look at the photoabsorption cross-section spectra in the ultraviolet region of wavelengths (Fig. 4), where the second collective dipole state shows up, it is noticed that the corresponding photoabsorption peaks are also fragmented for some clusters. For some clusters there exists only one peak

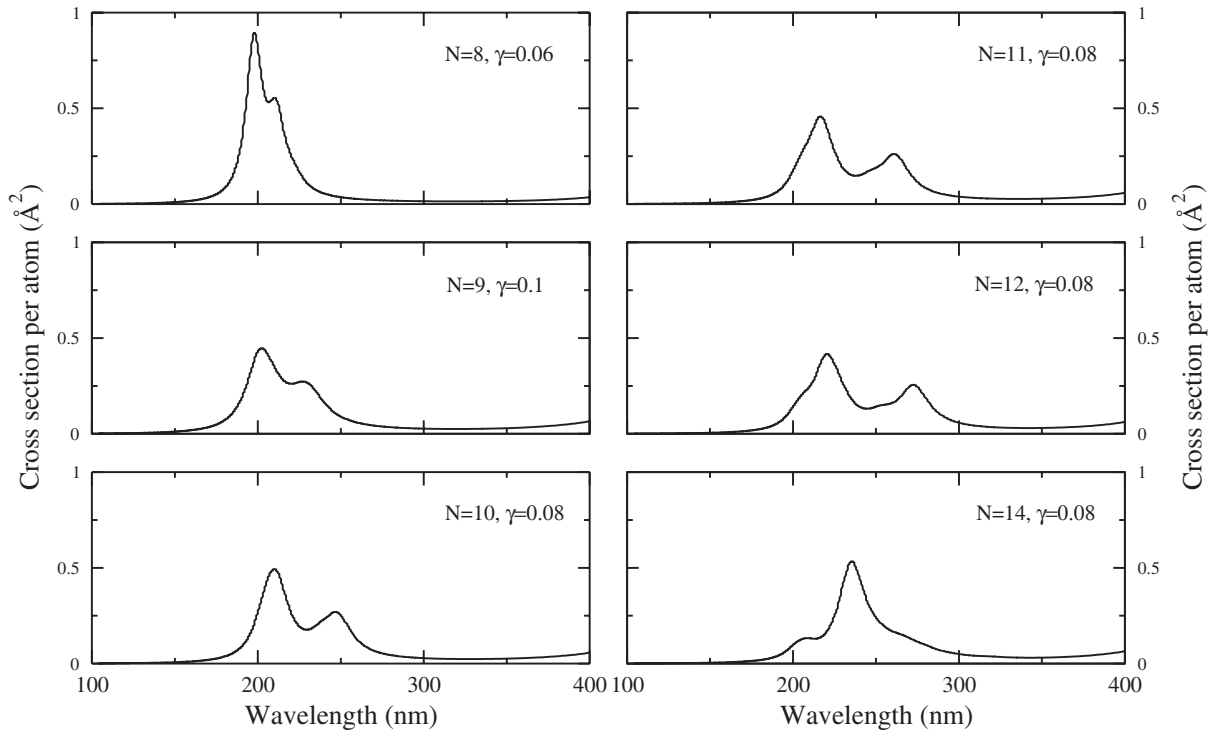


FIG. 4. Photoabsorption cross section vs wavelength for the second dipole collective state which can be associated with the volume plasma resonances.

in this wavelength domain and this happens due to the near spherical form of these clusters. Indeed, the single peak shape is caused by the fact that for spherical clusters there is only one collective state, while for strongly deformed clusters this state is split into two parts, one consisting of two degenerate states of energy $\hbar\omega_x = \hbar\omega_y$, and another one of energy $\hbar\omega_z$. The ordering of the two energies depends on the cluster shape. For prolate clusters $\omega_z \leq \omega_x$, while for oblate clusters the ordering is changed. It is natural to suppose that the highest peak corresponds to the double degenerate energies $\hbar\omega_x = \hbar\omega_y$. Keeping this picture in mind and inspecting the cross sections shown in Fig. 4, one can conclude that for most clusters with the second collective dipole states fragmented, the ordering of the larger and the smaller peaks suggests a prolate shape. By contrast, the cluster Na_{14} has an oblate shape. This reasoning agrees perfectly well with the experimental data. Also, it is known that Na_8 is a spherical cluster, which is reflected in a single almost degenerate peak of the second collective dipole state. The dependence of the plasmon profile on the cluster shape has been studied experimentally in Ref. [40]. Also the aforementioned features are consistent with the semiclassical results presented in Ref. [27]. Concluding, our analysis indicates that the cluster shape is reflected in the profiles of both surface and volume plasmons.

Comparing the surfaces covered by the curves in Fig. 4 and by the corresponding ones from Fig. 3, respectively, one may conclude that the volume plasmon takes only a small fraction of the dipole strength, which is in agreement with the result of Ref. [40] saying that the surface plasmon

exhausts about 70%–100% of the dipole sum rule. A detailed analysis of the two types of plasmons, surface and volume, has been given in Ref. [5]. Thus, the two plasmons are analogous to the Goldhaber-Teller and Steinwedel-Jensen modes of nuclear systems, respectively. The volume plasmon for large systems does not couple to the light and therefore cannot be populated. The reason is the fact that the light waves are transverse while plasma waves in infinite medium are longitudinal. In finite-sized particles, on the other hand, the volume mode can couple to light. The weight factors of the two modes' contributions to the photoabsorption cross section have been measured for some sodium clusters in Refs. [14,15,41]. Thus, the weights for the surface plasmon in Na_8 and Na_{20} are 0.7 ± 0.05 (Ref. [14]) and 0.7 ± 0.1 (Ref. [41]), respectively. Another type of experiment [15] predicts for the weight of the surface plasmon in Na_8 the value 0.64 ± 0.3 . The ratios of the aforementioned surfaces for the two small clusters are close to the corresponding experimental results given above. Thus, we may say that our results agree with the calculations of Kresin [42] which predict that the photoabsorption strength in neutral spherical Na clusters is shared between a surface- and a volume-plasma resonance.

In Fig. 5 theoretical estimations for the static electric polarizability per atom, normalized to the value of polarizability of neutral Na atom, are shown together with experimental values and LDA results for a few clusters. The three data sets are compared with one another as well as with the bulk limit result, which is associated with the classical polarizability of a metal sphere. An excellent agreement is obtained for most

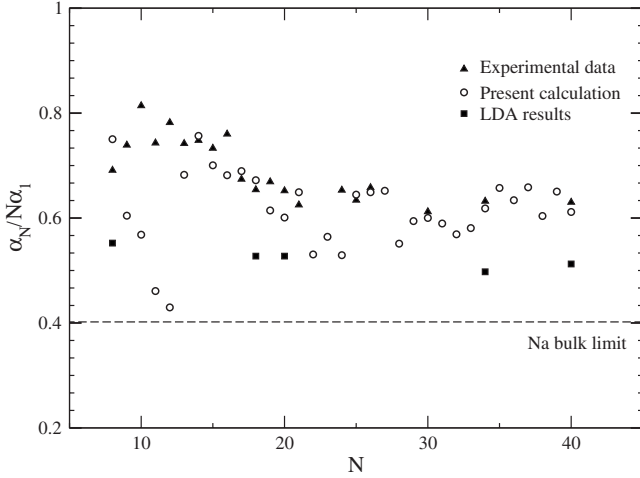


FIG. 5. The predicted static electric polarizabilities per atom for Na_N clusters normalized to the measured polarizability of Na atom (Ref. [43]) (open circles) are compared with the corresponding experimental data (black triangles) from Ref. [13] and with those given in Ref. [44] with a LDA approach. The bulk limit is also visualized.

clusters' polarizabilities. However, there are few cases where big discrepancies are recorded, namely, Na_9 , Na_{10} , Na_{11} , and Na_{12} . The noteworthy fact is that these clusters are mostly fragmented, some of them displaying a smooth two peak structure or even continuous plateaus of the photoabsorption cross-section spectrum.

It is fair to mention that the present work uses a temperature-independent formalism. However, according to Ref. [45] the temperature effect on the polarizability is relatively large. Indeed, the deviation of the measured polarizability at the room temperature from that corresponding to $T=0$ is about 15%. To this discrepancy one should add a correction due to the cluster shape thermal fluctuation which amounts to $\pm 3\%$. If one adds the temperature effects to the values plotted in Fig. 5, the agreement between the calculated values and the corresponding data will be improved for some clusters and moderately altered for the remaining ones.

VII. CONCLUSIONS

The main results described in the previous sections can be summarized as follows. The atomic clusters were replaced by a set of valence electrons moving in a mean field and interacting among themselves through a Coulomb and an exchange interaction. Although not presented analytically, the mean field is defined by a set of orthogonal projected spherical single-particle states and a set of corresponding energies. The two-body interaction is expanded in multipoles, the expansion being truncated at $\lambda=1$. The mean field and the two-body dipole interaction are treated within the RPA approach which defines a set of particle-hole-like phonon states. The $E1$ transition from the ground state to excited one-phonon states was calculated. The collective $E1$ transitions to the low-energy states, around 2.5 eV, are determined by a coherent contribution of the $\Delta N=1$, p - h configuration.

There are also states, of energies about 5 to 6 eV, which are collectively populated with $\Delta N=3$ p - h transitions. As shown in Fig. 2, the first collective mode has a surface character while the second one seems to be mainly of a volume type.

The photoabsorption cross section was obtained by folding the $E1$ strengths carried by the RPA one-phonon states, with Lorentzian with a damping factor varying from one cluster to another, in the range of 0.06–0.135. The result shown in Eq. (4.6) is plotted in Fig. 3 as a function of the wavelength associated with the RPA states, and compared with the experimental data. The comparison reveals a reasonably good agreement. For the light clusters, $N=9, 10, 11, 12$, the figures exhibit two peaks, which suggest the existence of two modes corresponding to oscillations along and perpendicular to the symmetry axis, respectively. For $N=14$, the results of our calculation indicate a triaxial shape. Similar fragmentation is also obtained for the volume plasmon resonance shown in Fig. 4. According to the relative magnitude of the two peaks, we concluded that the clusters with $N=9, 10, 11, 12$ have a deformed prolate shape while Na_{14} seems to be of an oblate shape. Perhaps a smaller damping factor would provide evidence for a triaxial shape also for the volume mode in Na_{14} .

It is noteworthy the fact that the fragmentation effects seen in both low-(surfacelike) and high-energy (volumelike) modes cannot be described with a spherical single-particle basis. Based on calculations for the number of spilled-out electrons, we calculated the electric polarizability which is compared with the experimental data, the bulk limit result as well as with the LDA predictions. Except for the clusters with $N=9, 10, 11, 12, 24$, the calculated polarizabilities agree quite well with the corresponding experimental data. It is interesting to remark that concerning the clusters for which large discrepancies were recorded, some of predictions ($N=9, 10, 24$) lie close to the LDA results while others ($N=11, 12$) agree with the bulk limit of Na clusters. Our formalism is a temperature-independent approach. Adding the temperature effect the picture shown in Fig. 5 would be modified, at the room temperature, by about 15% [45]. However, the corrected polarizabilities are still in a reasonable good agreement with the experimental data. The final conclusion is that the projected spherical single-particle basis seems to be a useful tool for describing the many-body features of deformed atomic clusters.

ACKNOWLEDGMENTS

This work was also supported by the Romanian Ministry for Education and Research under the contract PNII, Grant No. ID-33/2007.

APPENDIX

The two terms of the two-body potential $V(r_1, r_2; 1)$ determine the two following two-body matrix elements:

$$R(ph', hp') = R_1(ph', hp') + R_2(ph', hp'),$$

$$R_1(ph', hp') = \int_0^\infty \left[\int_0^{r_2} r_1^3 R_{n_p l_p}(r_1) R_{n_h l_h}(r_1) dr_1 \right] \\ \times R_{n_p' l_p'}(r_2) R_{n_h' l_h'}(r_2) dr_2, \\ R_2(ph', hp') = F(\rho, r_s) \int_0^\infty R_{n_p l_p}(r_1) R_{n_h l_h}(r_1) \\ \times R_{n_p' l_p'}(r_1) R_{n_h' l_h'}(r_1) r_1^2 dr_1. \quad (\text{A1})$$

The factors f involved in the RPA matrices have the expressions

$$f_{l_p l_h}^{I_p I_h}(d) = -\frac{1}{2} \nu(I_p) \nu(I_h) \mathcal{N}_{n_p l_p}^{I_p}(d) \mathcal{N}_{n_h l_h}^{I_h}(d) [N_{l_p+1}^{(c)}]^{-2} \frac{1}{\sqrt{2l_p+3}} \\ \times C_{000}^{l_h 1 l_p} C_{l_h 0 l_h}^{l_h l_p+1 I_h}; W(1 l_p I_h l_h; l_p+1 1), \quad (\text{A2})$$

for $(I_p, l_p) = (0, \text{odd})$ and $(I_h, l_h) \neq (0, \text{odd})$,

$$f_{l_p l_h}^{I_p I_h}(d) = \frac{1}{2} \nu(I_p) \nu(I_h) \mathcal{N}_{n_p l_p}^{I_p}(d) \mathcal{N}_{n_h l_h}^{I_h}(d) [N_{l_h+1}^{(c)}]^{-2} \frac{1}{\sqrt{2l_h+3}} \\ \times C_{000}^{l_h 1 l_p} C_{l_p 0 l_p}^{l_h+1 I_p} W(1 l_h I_p l_p; l_h+1 1), \quad (\text{A3})$$

for $(I_h, l_h) = (0, \text{odd})$ and $(I_p, l_p) \neq (0, \text{odd})$,

$$f_{l_p l_h}^{I_p I_h}(d) = \nu(I_p) \nu(I_h) \mathcal{N}_{n_p l_p}^{I_p}(d) \mathcal{N}_{n_h l_h}^{I_h}(d) \\ \times \sum_J C_{l_p 0 l_p}^{l_p J I_p} C_{l_h 0 l_h}^{l_h J I_h} [N_J^{(c)}]^{-2} W(I_h J 1 l_p; l_h I_p), \quad (\text{A4})$$

for $(I_p, l_p) \neq (0, \text{odd})$ and $(I_h, l_h) \neq (0, \text{odd})$, where $\nu(I_i) = \frac{2-\delta_{i,0}}{2I_i+1}$ is the statistical factor connected to the fact that the energy level with a given I has the degeneracy $2I+1$ and it contains also the $I, -I$ degeneracy which adds a factor 2 if $I \neq 0$. The Clebsch-Gordon coefficients appearing in the above expressions take proper care of the angular momentum coupling, as well as of the parity-conservation conditions.

-
- [1] W. D. Knight, K. Clemenger, W. A. de Heer, W. A. Saunders, M. Y. Chou, and M. L. Cohen, *Phys. Rev. Lett.* **52**, 2141 (1984).
[2] G. Galli and M. Parrinello, in *Computer Simulations in Materials Science*, NATO Advanced Studies Institute, Series E: Applied Science Vol. 205, edited by M. Meyer and V. Pontikis (Kluwer, Dordrecht, 1991), p. 283.
[3] W. A. de Heer, *Rev. Mod. Phys.* **65**, 611 (1993).
[4] M. Brack, *Rev. Mod. Phys.* **65**, 677 (1993).
[5] V. V. Kresin, *Phys. Rep.* **220**, 1 (1992).
[6] M. Cini, *J. Catal.* **37**, 187 (1975).
[7] V. Bonačić-Koutecký, P. Fantucci, and J. Koutecký, *Phys. Rev. B* **37**, 4369 (1988).
[8] W. Kohn and L. J. Sham, *Phys. Rev.* **140**, A1133 (1965).
[9] J. L. Martins, J. Buttet, and R. Car, *Phys. Rev. B* **31**, 1804 (1985).
[10] D. E. Beck, *Solid State Commun.* **49**, 381 (1984).
[11] H. Nishioka, K. Hansen, and B. R. Mottelson, *Phys. Rev. B* **42**, 9377 (1990).
[12] M. Y. Chou and M. L. Cohen, *Solid State Commun.* **52**, 645 (1984).
[13] K. Selby, M. Vollmer, J. Masui, V. Kresin, W. A. de Heer, and W. D. Knight, *Phys. Rev. B* **40**, 5417 (1989).
[14] K. Selby, V. Kresin, J. Masui, M. Vollmer, W. A. de Heer, A. Scheidemann, and W. D. Knight, *Phys. Rev. B* **43**, 4565 (1991).
[15] C. Brechignac, Ph. Cahuzac, F. Carlier, M. de Frutos, and J. Leygnier, *Chem. Phys. Lett.* **189**, 28 (1992).
[16] H. Fallgren, K. M. Brown, and T. P. Martin, *Z. Phys. D: At., Mol. Clusters* **19**, 81 (1991).
[17] C. Yannouleas and R. A. Broglia, *Phys. Rev. A* **44**, 5793 (1991).
[18] C. Yannouleas and Uzi Landman, *Phys. Rev. B* **51**, 1902 (1995).
[19] M. Koskinen, P. O. Lipas, and M. Manninen, *Z. Phys. D: At., Mol. Clusters* **35**, 285 (1995).
[20] K. Clemenger, *Phys. Rev. B* **32**, 1359 (1985).
[21] S. G. Nilsson, K. Dan. Vidensk. Selsk. Mat. Fys. Medd. **29** (1955), No. 16.
[22] A. A. Raduta, Ad. R. Raduta, and Al. H. Raduta, *Phys. Rev. B* **59**, 8209 (1999).
[23] J. Pedersen, S. Bjornholm, J. Borggreen, K. Hansen, T. P. Martin, and H. D. Rasmussen, *Nature (London)* **353**, 733 (1991).
[24] T. P. Martin, S. Bjornholm, J. Borggreen, C. Brechignac, Ph. Cahuzac, K. Hansen, and J. Pedersen, *Chem. Phys. Lett.* **186**, 53 (1991).
[25] M. Koskinen, P. O. Lipas, and M. Manninen, *Nucl. Phys. A* **591**, 421 (1995).
[26] A. Rigo, M. Casas, F. Garcias, E. Moya de Guerra, and P. Sarriguren, *Phys. Rev. B* **57**, 11943 (1998).
[27] A. A. Raduta, E. Garrido, and E. Moya de Guerra, *Eur. Phys. J. D* **15**, 65 (2001).
[28] A. A. Raduta, D. S. Delion, and N. Lo Iudice, *Nucl. Phys. A* **551**, 93 (1993).
[29] A. A. Raduta, A. Escuderos, and E. Moya de Guerra, *Phys. Rev. C* **65**, 024312 (2002).
[30] O. Gunnarsson and B. I. Lundqvist, *Phys. Rev. B* **13**, 4274 (1976).
[31] W. Ekardt, *Phys. Rev. B* **29**, 1558 (1984).
[32] M. Brack, *Phys. Rev. B* **39**, 3533 (1989).
[33] N. Ullah and D. J. Rowe, *Nucl. Phys. A* **163**, 257 (1971).
[34] V. Zelevinsky, A. Volya, and N. Auerbach, *Phys. Rev. C* **78**, 014310 (2008).
[35] J. M. Pacheco and R. A. Broglia, *Phys. Rev. Lett.* **62**, 1400 (1989).
[36] G. F. Bertsch and D. Tomanek, *Phys. Rev. B* **40**, 2749 (1989).

- [37] C. Yannouleas and R. A. Broglia, *Phys. Rev. A* **44**, 5793 (1991).
- [38] N. Van Giai, *Progress of Theoretical Physics, Supplement No.124* (1996) 1.
- [39] G. Mie, *Ann. Phys.* **25**, 377 (1908).
- [40] J. Borggreen, P. Chowdhury, N. Kebaili, L. Lundsberg-Nielsen, K. Lutzenkirchen, M. B. Nielsen, J. Pedersen, and H. D. Rasmussen, *Phys. Rev. B* **48**, 17507 (1993).
- [41] S. Pollack, C. R. C. Wang, and M. M. Kappes, *J. Chem. Phys.* **94**, 2496 (1991).
- [42] V. Kresin, *Phys. Rev. B* **42**, 3247 (1990).
- [43] R. W. Molof, H. L. Schwartz, T. M. Miller, and B. Bederson, *Phys. Rev. A* **10**, 1131 (1974).
- [44] S. M. Reimann, M. Koskinen, H. Hakkinen, P. E. Lindelof, and M. Manninen, *Phys. Rev. B* **56**, 12147 (1997).
- [45] S. A. Blundell, C. Guet, and R. R. Zope, *Phys. Rev. Lett.* **84**, 4826 (2000).